A Photolysis-Triggered Heme Ligand Switch in H93G Myoglobin†

Stefan Franzen,*,‡ James Bailey,§ R. Brian Dyer,§ William H. Woodruff,§ Robert B. Hu,|| Melissa R. Thomas,|| and Steven G. Boxer||

Department of Chemistry, North Carolina State University, Raleigh, North Carolina 27695-8204, Bioscience and Biotechnology Group, Los Alamos National Laboratory, Los Alamos, New Mexico 87545, and Department of Chemistry, Stanford University, Stanford, California 94305

Received October 5, 2000; Revised Manuscript Received February 14, 2001

ABSTRACT: Resonance Raman spectroscopy and step-scan Fourier transform infrared (FTIR) spectroscopy have been used to identify the ligation state of ferrous heme iron for the H93G proximal cavity mutant of myoglobin in the absence of exogenous ligand on the proximal side. Preparation of the H93G mutant of myoglobin has been previously reported for a variety of axial ligands to the heme iron (e.g., substituted pyridines and imidazoles) [DePillis, G., Decatur, S. M., Barrick, D., and Boxer, S. G. (1994) *J. Am. Chem. Soc. 116*, 6981−6982]. The present study examines the ligation states of heme in preparations of the H93G myoglobin with no exogenous ligand. In the deoxy form of H93G, resonance Raman spectroscopic evidence shows water to be the axial (fifth) ligand to the deoxy heme iron. Analysis of the infrared C−O and Raman Fe−C stretching frequencies for the CO adduct indicates that it is six-coordinate with a histidine trans ligand. Following photolysis of CO, a time-dependent change in ligation is evident in both step-scan FTIR and saturation resonance Raman spectra, leading to the conclusion that a conformationally driven ligand switch exists in the H93G protein. In the absence of exogenous nitrogenous ligands, the CO trans effect stabilizes endogenous histidine ligation, while conformational strain favors the dissociation of histidine following photolysis of CO. The replacement of histidine by water in the five-coordinate complex is estimated to occur in $<5\ \mu$s. The results demonstrate that the H93G myoglobin cavity mutant has potential utility as a model system for studying the conformational energetics of ligand switching in heme proteins such as those observed in nitrite reductase, guanylyl cyclase, and possibly cytochrome *c* oxidase.

In heme proteins both ligand conformation and electrostatic environment provide a mechanism to control the reactivity of the heme iron. Strain in the proximal histidine conformation, coupled to protein structure, modulates the binding affinity of diatomic ligands CO, NO, and O_2 to the distal side of the heme. The binding of these ligands, in turn, affects the binding affinity of the histidine for the heme iron. For example, the backbone geometry in the T state of hemoglobin (Hb)[1] induces strain on the proximal histidine, thereby reducing the binding affinity of CO and O_2 (*2*). In effector-induced T-state Hb, NO binding to the heme iron weakens the iron−histidine bond to the point of rupturing the proximal histidine−iron bond in the α subunits (*3*). The trans effect of NO has functional consequences in soluble guanylyl cyclase (sGC) where the proximal Fe−His bond is ruptured by NO binding (*4*, *5*). Although the best documented functional ligand switch events involve NO (*4*−*6*), a role for CO has been proposed in cytochrome *c* oxidase (*7*).

Resonance Raman spectroscopy has been used to determine the strength of binding interactions between the heme iron and the histidine ligand in proteins. The frequency of the iron−histidine band in the 200−245 cm^{-1} region has been shown empirically to be proportional to bond length and to be indicative of changes in bond strength, including rupture of the Fe−His bond (*8*, *9*). For example, the lengthening of the Fe−His bond associated with the transition from hemoglobin R to T quaternary structures is reflected in a lowering of ν(Fe−His) from 225 to 216 cm^{-1} (*10*, *11*). In sGC, the lability of the Fe−His bond upon NO binding is evident in a lower frequency of the Fe−His band of the deoxy form of sGC compared to globins (9). The resonance Raman band in this region of the spectrum is absent if very weakly bound histidine is replaced by H_2O or another weak ligand in the five-coordinate heme−iron adduct as shown for the cavity mutant of heme oxidase, H25A (*12*).

Studies of the enzyme cytochrome *c* oxidase (CcO) demonstrate that changes in the ligation of the heme−copper binuclear center are important for the function of complex redox-linked proton pumps (*7*, *13*). CcO shows a change in frequency of ν(Fe−His) from 214 cm^{-1} in equilibrium deoxy CcO to 222 cm^{-1} in the CcO−CO photoproduct (*13*). The change in frequency of ν(Fe−His) may reflect proximal control over oxygen ligation as in Hb. However, the observed spectral dynamics could be due to a ligation switch as in the case of sGC (*7*). The ligation states possible in complex

† This work was supported in part by a grant to S.G.B. from the NIH (GM27738) and to S.F. from the NSF (MCB-9874895).

* To whom correspondence should be addressed. Phone: (919)-515-8915. Fax: (919)-515-8909. E-mail: Stefan_Franzen@ncsu.edu.

‡ North Carolina State University.

§ Los Alamos National Laboratory.

|| Stanford University.

[1] Abbreviations: FTIR, Fourier transform infrared; CO, carbon monoxide; NO, nitric oxide; sGC, soluble guanylyl cyclase; Hb, hemoglobin; Mb, myoglobin; CcO, cytochrome *c* oxidase; THF, tetrahydrofuran.

10.1021/bi0023403 CCC: $20.00
Published on Web 04/06/2001

systems such as CcO can be addressed through study of an appropriate protein model system. In this paper we present evidence that the strength of ligand binding interactions and the role of protein conformation in determining the ligation of histidine or other heme iron ligands can be addressed using the proximal cavity mutant of myoglobin, H93G (*1*, *14*, *15*). Ligand switching is a general phenomenon observed in a range of heme proteins. For example, CooA is a transcriptional activator triggered by heme-centered ligand switch coupled to CO binding to the heme iron (*16*−*19*).

The H93G mutant consists of the substitution of the proximal histidine by glycine (*14*). The cavity created by the H93G mutation can be filled with a variety of heterocyclic ligands (L), allowing a comparison of properties as a function of ligand basicity or ligand conformation in deoxy H93G(L), H93G(L)CO, or H93G(L)NO complexes (*1*, *20*). In the present study, we address the properties of H93G prepared in the absence of exogenous heterocyclic ligands, i.e., with no imidazole in the proximal cavity. Preparations in which deoxy heme is present, but no nitrogenous ligand has been added, are designated H93G. These preparations are distinguished from those formed by the addition of an imidazole or other heterocyclic ligand to form the deoxy adduct H93G(L). Using this abbreviation the heme adducts in H93G can be expressed as H93G(H_2O) and H93G(His) for the deoxy heme five-coordinate adducts of water and endogenous histidine, respectively. Similarly, the CO adducts are H93G(H_2O)CO and H93G(His)CO. The data presented in this paper show that, in the absence of heterocyclic ligands, a five-coordinate adduct, H93G(His), is still formed. Upon photolysis of H93G(His)CO, a change in ligation occurs, forming a transient five-coordinate intermediate, H93G(H_2O). The rapid dynamic ligand switch indicated by the data provides insight into heme dynamics relevant to proteins where a balance of forces gives rise to weak histidine ligation.

EXPERIMENTAL PROCEDURES

The H93G mutant was obtained by applying cassette mutagenesis to the sperm whale myoglobin gene in the plasmid pMb413b as described previously (*14*). The double mutant H64V/H93G was constructed by introducing a random mutation at position H64 into the H93G mutant in pMb413b plasmid. A single random codon cassette 36 base pairs in length was designed to mutate H64 from CAT to DBN where D = AGT, B = CGT, and N = ACGT (*21*) The randomized plasmid was transformed into competent BL21 (lambda DE3) *Escherichia coli* and grown in 2YT media with 10 mM concentration of exogenous imidazole (Im) as has been discussed elsewhere (*1*). Standard protein purification techniques were used for the mutant proteins, although the protein yield was lower for the double mutation H64V/H93G.

We have examined several preparations of H93G in the absence of exogenous heterocyclic ligand. Extensive dialysis against ligand-free buffer (50−100 mM phosphate, pH 7) does not appear to remove all of the ligand from H93G(Im) (*21*). Both resonance Raman and NMR (data not shown) indicate the presence of two populations [one of which is H93G(Im)] despite extensive dialysis. The difficulty in removing imidazole may be due to isolation of the H93G protein as an equal mixture of ferric metaquo and oxy forms. On the basis of the observed CO trans effect (*22*) it is possible that the binding constant for imidazole in the oxy form is much larger than in the ferric metaquo form. To remove the oxy H93G(Im) impurity in dialyzed samples, 1 mM ferricyanide was added to H93G(Im). Excess ferricyanide was removed on a G-25 Sephadex size exclusion column, and the protein was extensively dialyzed against ligand-free buffer. Preparations of this type consisted of 80−90% H93G, but there was a remaining H93G(Im) impurity detectable by resonance Raman spectroscopy. Although the oxidation of protein produced significantly better results than dialysis alone, it has not proven possible to obtain completely pure exogenous-ligand-free H93G by the above methods. To obtain preparations of H93G without any detectable imidazole ligand, we extracted heme from the protein, followed by dialysis, reconstitution with heme, and further dialysis (*23*).

Continuous wave resonance Raman spectra were obtained using an argon ion pumped Coherent dye laser with Stilbene 420 dye. Typical laser powers at the sample ranged from 5 to 20 mW focused to a ≈100 μm beam waist using a cylindrical focus. A 135° backscattering geometry was used, and the polarization was scrambled prior to entering the monochromator. Excitation wavelengths of 422.2−424.0 and 429.5−432.0 nm were used for experiments on six-coordinate CO-ligated heme proteins and five-coordinate heme proteins, respectively. The H93G-CO and H93G/H64V-CO samples were spun at 300 Hz in a spinning sample cell. A SPEX 0.6 m triplemate monochromator was used to disperse the collected light onto a Photometrics CCD with a resolution of 2.5 cm^{-1}. Raman experiments were performed on samples containing ≈100 μM protein in 0.1 M sodium phosphate buffer, pH 7.0. Ferrous H93G and H93G(Im) samples were prepared by addition of a minimum volume of 1 M dithionite to N_2-degassed protein solutions. The ferrous H93G-CO form was prepared by equilibrating deoxy H93G samples with 0.1 atm of CO.

Fourier transform infrared (FTIR) spectra were obtained using a Bio-Rad FTS 60. Step-scan spectra were obtained with 5 μs time resolution using an external cavity with focusing optics of local design (*24*). Protein samples were concentrated by diafiltration to approximately 800 μM in 0.1 M sodium phosphate buffer, pH 7.0. Concentrated protein solutions were reduced with 1 M dithionite, equilibrated with CO, and loaded into a purged, sealed solution cell composed of CaF_2 windows separated by a 50 μm spacer. The sample was photoexcited by a Spectra-Physics DCR-11 YAG laser with doubled output at 532 nm and with a 10 ns pulse duration at a 10 Hz repetition rate. A DG535 digital delay generator controlled timing of the laser Q-switch with respect to displacement of the mirror in the interferometer. Laser pulses of 1 mJ were focused to a 100 μm beam waist in a sample compartment external to the FTIR bench.

RESULTS

The low-frequency regions of the resonance Raman spectra for deoxy ferrous H93G and H93G(Im) are shown in Figure 1. For deoxy H93G(Im) the iron−histidine axial out-of-plane mode is observed at 225 cm^{-1} and exhibits an isotopic shift of ≈0.9 cm^{-1} upon substitution of d_3-imidazole into the

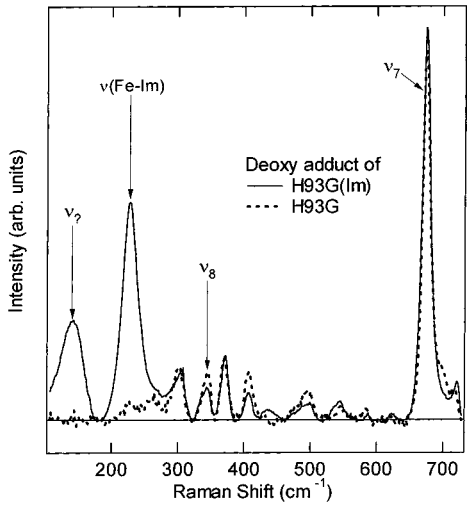

FIGURE 1: Figure 1. Resonance Raman spectra of deoxy H93G-(Im) (solid line) and deoxy H93G (dotted line). The low-frequency region of the spectrum is shown for 430 nm excitation at ambient temperature. The Raman band at 225 cm^{-1} in the H93G(Im) spectrum has been shown to be a mode with a significant iron−imidazole stretching character, ν(Fe−His). Both this band and the unassigned band at 150 cm^{-1}, denoted $\nu_?$, are absent in the deoxy H93G spectrum. The spectra were normalized to the ν_7 band at 672 cm^{-1}.

proximal ligand binding cavity (*25*). This frequency agrees with the iron−histidine axial out-of-plane vibrational mode assigned for deoxy myoglobin at 218−220 cm^{-1} (*26*, *27*). This mode is apparently absent for deoxy H93G. The high-frequency Raman spectra of deoxy H93G, H93G(Im), and wild-type myoglobin are essentially identical, indicating that deoxy H93G is a five-coordinate high-spin heme adduct even in the absence of imidazole. The ν_3 mode is observed at 1470 ± 2 cm^{-1} and is indicative of a high-spin five-coordinate complex. The electron density marker, ν_4, is observed at 1357 ± 2 cm^{-1} and suggests the absence of strain in the axial ligation to the deoxy heme iron (Supporting Information).

In the resonance Raman spectrum of deoxy H93G shown in Figure 1 there are no observable bands below 230 cm^{-1}. This result suggests that both the iron−ligand axial out-of-plane mode and the unassigned resonance Raman band at 150 cm^{-1} arise only for heterocyclic ligand adducts.[2] The absence of these Raman bands in deoxy H93G is significant since they are observed in the resonance Raman spectra of all histidine-ligated deoxy proteins and deoxy H93G(L) samples, where L represents a variety of substituted pyridines and imidazoles (*25*). The resonance Raman spectrum in Figure 1 is similar to that of the H25A mutant of heme oxygenase, which lacks a histidine ligand to the heme iron (*12*). The absence of the iron−ligand axial out-of-plane mode in a five-coordinate Raman spectrum indicates that a non-nitrogenous ligand is in the fifth coordinate position.

To determine the identity of the axial ligand in H93G, the CO adduct was prepared. A shift in the Soret absorption spectrum is observed from λ_{max} = 420 nm for H93G(Im)-CO to λ_{max} = 418 nm for H93G-CO. The resonance Raman data shown in Figure 2 suggest that the Fe−C stretch is composed of three components at approximately 490, 507, and 520 cm^{-1}. The line shape of the Fe−C band is asymmetric, and the spectrum H93G-CO shown in Figure 2 has the same shape as H93G(Im)CO and MbCO. Because the ratio of the intensities of the 490 cm^{-1} band to the 507 cm^{-1} band is constant in all species where it is observed, the 490 cm^{-1} band will be ignored until the Discussion section where a quantitative analysis is carried out. For comparison, the spectra obtained with different intensities were normalized at the ν_7 Raman band. The frequency of the majority component depends on the intensity of the Raman laser beam and shifts from a peak at 507 cm^{-1} to 520 cm^{-1} as the laser intensity is increased. The changes with laser intensity were fully reversible. The intensity dependence of H93G-CO contrasts with the Fe−C stretch at 507 cm^{-1} for both wild-type MbCO and H93G(Im)CO. Under low photolysis the CO-bound states of MbCO and H93G(Im)CO are observed while at high laser intensities, the observed photoproducts are deoxy Mb and deoxy H93G(Im), respectively. The Fe−C frequencies remain at 507 cm^{-1} independent of laser intensity (see, for example, the lowest spectrum of wild-type MbCO in Figure 2).[3] The observed intensity dependence of the Fe−C stretch in H93G-CO differs from MbCO and H93G-(Im)CO data in that the Fe−C band changes shape. The presence of more than one species or photoproduct suggests

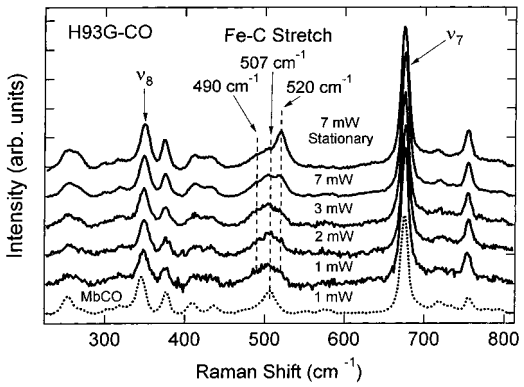

FIGURE 2: Resonance Raman spectra of H93G-CO under varying excitation intensity. The low-frequency region of the spectrum is shown for 422.2 nm excitation at ambient temperature. The photolysis rate of the laser corresponds to ≈3 × 10^{-3} s^{-1}/mW.[6] The spectral difference in the intensities of the 507 and 520 cm^{-1} Raman bands upon increasing laser photolysis indicates the presence of a photolyzed intermediate. The high-frequency region is identical under all photolysis conditions (data not shown), indicating that the intermediate species is a six-coordinate CO adduct of H93G as is the equilibrium species. The comparison spectrum of wild-type MbCO (dashed line) was obtained at 1 mW excitation laser intensity in a spinning cell.

[2] The 150 cm^{-1} mode observed in deoxy wild-type myoglobin and in deoxy H93G(L) for a variety of ligands has a depolarization ratio similar to that observed in deoxy H93G(Im) ($\rho \approx 0.4$). Although this mode has never been assigned, it clearly depends on the identity of the axial ligand.

[3] The classic π-back-bonding correlation suggests an inverse correlation between Fe−CO and C−O stretching frequencies, Fe−CO (490 cm^{-1}) → C−O (1963 cm^{-1}), Fe−CO (507 cm^{-1}) → C−O (1945 cm^{-1}), and Fe−CO (520 cm^{-1}) → C−O (1936 cm^{-1}). However, this correlation is applicable to globins and model systems that have a neutral imidazole ligand. The Fe−CO and C−O frequencies shift to lower values in parallel in peroxidases and to higher values in parallel in cytochrome *c* oxidase due to a σ-bond contribution from the proximal ligand. Here we can point to an experimental correlation that suggests that the 520 cm^{-1} band in the photoproduct Raman spectra (Figure 2) is correlated with the band 1960 cm^{-1} of the intermediate observed by the step-scan FTIR experiment (Figure 3). These values are consistent with a the change in proximal ligation in the photoproduct.

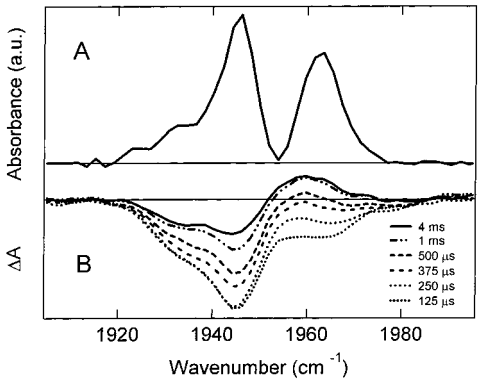

FIGURE 3: (A) Fourier transform infrared spectra of H93G-CO at ambient temperature. The spectra were obtained on a large D_2O background. The baseline of the background was subtracted to obtain a flat baseline in the region of the three C−O bands observed at 1936, 1945, and 1963 cm^{-1}. (B) Step-scan FTIR difference spectra showing the CO stretching region at various times after photolysis. The CO stretching frequency at equilibrium is shown in the top spectrum. Difference spectra are shown at 125 μs, 250 μs, 375 μs, 500 μs, 1 ms, and 4 ms.

a light-driven change in the ligation state of the six-coordinate CO adduct to a species with an Fe−C stretch at about 520 cm^{-1}. This light-driven change is not observed in H93G(Im)CO.

To elucidate the nature of the six-coordinate adduct formed by laser photolysis of H93G-CO, we studied the photolysis process by step-scan FTIR with 5 μs time resolution. The equilibrium FTIR spectrum of H93G-CO consists of three IR bands at 1936, 1945, and 1963 cm^{-1} shown in Figure 3A. Figure 3B depicts the change in CO frequency during the 125 μs to 4 ms time scale following photolysis of CO from H93G-CO. In the 125 μs FTIR difference spectrum, the bleach consists of a reduction in infrared absorption intensity in all three bands, with an apparently more rapid recombination occurring in the population at 1963 cm^{-1} compared to the populations at 1936 and 1945 cm^{-1}. By 1 ms, the difference spectrum has the appearance of a CO stretching difference with a positive lobe at 1960 cm^{-1} and negative lobes at 1936 and 1945 cm^{-1}. The 1960 cm^{-1} lobe does not correspond exactly to any of the frequencies in the equilibrium FTIR spectrum. The difference spectrum indicative of a change in ligation changes slightly between 1 and 4 ms but is still present at a time much longer than typical for bimolecular recombination in H93G(Im)CO or MbCO (Supporting Information). The equilibrium species is characterized by three FTIR bands in the C−O stretching region at 1936, 1945, and 1963 cm^{-1} that may be associated with the three Raman bands at 490, 507, and 520 cm^{-1} in the Fe−C stretch.[3] Step-scan FTIR spectra of H93G(Im)CO show a behavior similar to that of wild-type MbCO. There is no observable change in frequencies of the Fe−CO stretching band during the CO recombination process (see Supporting Information). The double mutant H93G/H64V was studied to test the hypothesis that the distal histidine, H64, can serve as the ligand to the heme iron of H93G in the absence of exogenous ligand. Since H64 is absent in this mutant, the distal histidine cannot serve as the fifth ligand in deoxy H93G/H64V or the sixth ligand in H93G/H64V-CO. The H93G/H64V protein was prepared in ligand-free form by heme extraction. By adding CO and a slight excess of dithionite, the CO complex was formed without

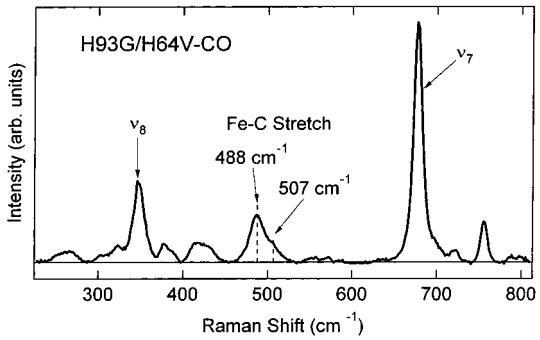

FIGURE 4: Resonance Raman spectra of the carbonmonoxy form of the H93G/H64V Mb mutant. The low-frequency region of the spectrum is shown for 423.1 nm excitation at ambient temperature. The Fe−C stretching mode is indicated at 488 cm^{-1} with a small band at 507 cm^{-1}. The data shown are an excitation intensity of 10 mW in a cell spinning at 300 Hz. Spectra obtained at powers as low as 1 mW and in a stationary cell were essentially identical.

any evidence of precipitated protein or free heme. The resonance Raman spectrum of H93G/H64V-CO shown in Figure 4 is similar to that of H93G-CO except that the Fe−C stretch was observed at 488 cm^{-1}, independent of laser intensity and spinning rate of the sample. The Fe−C frequency observed in the H93G/H64V double mutant is consistent with data for a variety of myoglobin mutants in which substituting hydrophobic residues for the distal histidine results in Fe−C frequencies in the 480−490 cm^{-1} range due to electrostatic effects (*28*).

DISCUSSION

On the basis of characteristic high-frequency Raman marker bands, such as the electron density marker, ν_4, and the core size region, ν_2, ν_3, and ν_{10} that are identical in deoxy Mb, deoxy H93G(Im), and deoxy H93G, we conclude that deoxy H93G is a five-coordinate complex. However, the low-frequency resonance Raman spectrum (Figure 1) indicates the lack of ligation by histidine or other heterocyclic ligands. Comparison with literature spectra suggests the fifth ligand to the heme iron can only be water, phosphate, or an amino acid side chain such as tyrosine, serine, or glutamate (*12*). In contrast, both the resonance Raman and the step-scan FTIR spectra of the H93G-CO six-coordinate adduct (Figures 2 and 3, respectively) are consistent with the presence of a histidine ligand at equilibrium. The Fe−C stretch at 507 cm^{-1} and CO stretch at 1945 cm^{-1} are very similar to frequencies observed in wild-type MbCO and in H93G(Im)CO. The difference in the axial ligation of the heme iron in the deoxy and CO forms indicates that the H93G protein may switch axial ligands upon CO dissociation. This hypothesis provides an explanation for time-dependent changes in the spectra observed following CO photolysis. In the following, we discuss the kinetic implications of a ligand switch and consider the conformational aspects that are important for the observed phenomenon. Figure 5 shows a general kinetic scheme that applies for an endogenous His ligand in competition for the heme iron with an exogenous ligand represented by H_2O.

Spectroscopic Assignment of the Ligands Involved in the Dynamic Switch. The resonance Raman and step-scan FTIR data show two distinct spectral features for the photoproduct of H93G-CO. As stated above, the Fe−C stretching fre-

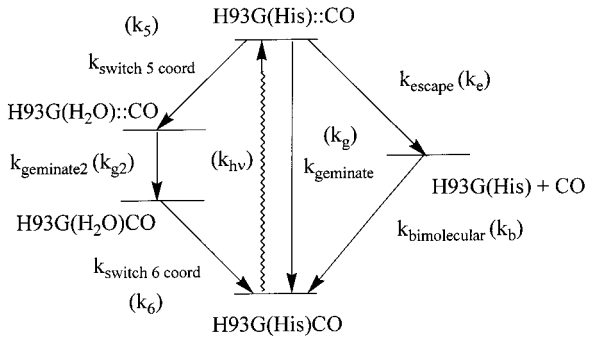

FIGURE 5: Rate scheme for photolysis of H93G-CO. The proposed structure of H93G-CO is H93G(His)CO with His97 ligated to the heme iron. Upon photolysis the species H93G(His)::CO has three possible channels, geminate recombination with rate constant $k_{geminate}$ (k_g), ligand escape to H93G(His) + CO with rate constant k_{escape} (k_e), or dissociation of H97 to form H93G(H_2O)::CO. In order for the ligand switch to be observed, the rate constant $k_{switch\ 5-coord}$ (k_5) must be significantly more rapid than either k_g or k_e. CO recombination in the geminate pair H93G(H_2O)::CO is rapid, giving rise to H93G(H_2O)CO, which lives for several milliseconds. The rate constant for geminate rebinding in this case is $k_{geminate2}$ (k_{g2}). The rate constant for bimolecular recombination is k_b, and the rate constant for the ligand switch H93G(H_2O)CO → H93G(His)CO is $k_{switch\ 6-coord}$ (k_6).

quency of 507 cm^{-1} and corresponding CO stretching frequency of 1945 cm^{-1} are consistent with a histidine-ligated species (*8*, *15*, *29*−*31*). Since the proximal histidine H93 is absent, there are two strong candidates for histidine ligation: H64 on the distal side and H97 on the proximal side. The photoproduct species has Fe−C and CO stretching frequencies of 520 and 1960 cm^{-1} similar to those of H93G(H_2O)CO. However, this combination of frequencies is also observed in cytochrome *c* oxidase, which has a histidine ligand (*8*, *29*). The resonance Raman data for deoxy H93G suggest that the stable five-coordinate heme adduct involves a nonheterocyclic ligand. For this reason, H93G(H_2O)CO is favored.

A correlation of the Fe−C and CO frequencies has been invoked using a bonding model that includes both π- and σ-bonding between the ligand and heme iron (*8*). Axial ligands that strengthen the π-interaction between a metal and CO produce a strong Fe−C bond, simultaneously weakening the C−O bond by adding electron density to the CO π^* antibonding orbital. However, strong trans σ-donors lead to parallel changes in the Fe−C and C−O stretching frequencies. For example, imidazolate weakens both the Fe−C bond and the C−O bond leading to the decrease in both stretching frequencies observed in cytochrome *c* peroxidase (*32*). Weak σ-donors produce the opposite effect, leading to stronger bonding in both Fe−C and CO. Compared to Fe−C Raman and FTIR CO bands of H93G-CO, H93G(Im)CO and MbCO at 507 and 1945 cm^{-1}, respectively, for all three species, *both* the Fe−C (520 cm^{-1}) and C−O (1960 cm^{-1}) frequencies are greater in the photoproduct, suggesting that σ-bonding is weaker (*8*). The Fe−C and CO stretching frequencies of 520 and 1960 cm^{-1}, respectively, also correspond to model complexes in which H_2O or THF is the trans ligand to CO. Thus, we assign the 1 ms photoproduct spectrum as H93G(H_2O)CO, depicted as the transient intermediate in Figure 5 (*33*, *34*).

Analysis of the Saturation Resonance Raman Spectra. A kinetic analysis was used to determine the quantum yield of formation of the photoproduct observed by resonance Raman (Figure 2) and step-scan FTIR (Figure 3) experiments based on the rate scheme shown in Figure 5. At equilibrium, the ligand in the six-coordinate CO adduct is histidine, designated H93G(His)CO. Photolysis of H93G(His)CO [ν(Fe−C) = 507 cm^{-1}, ν(C−O) = 1945 cm^{-1}] leads to H93G(His)::CO, where CO remains in the proximal pocket of the protein, but the heme is a five-coordinate species. The His ligand is replaced by H_2O via the process designated $k_{switch5}$ (k_5) to give H93G(H_2O)::CO. The intermediate H93G(H_2O)::CO is not observed in the transient spectra, but its spectrum is presumed to be similar to that shown in Figure 1 for H93G (i.e., no Fe−L stretch because the axial ligand is H_2O). The CO ligand recombines to form six-coordinate H93G(H_2O)CO [ν(Fe−C) = 520 cm^{-1}, ν(C−O) = 1960 cm^{-1}] with rate constant $k_{geminate2}$ (k_{g2}). In a final rate-limiting step, with rate constant $k_{switch6}$ (k_6), the H_2O trans ligand is replaced by His to re-form H93G(His)CO.

Since the ligand switch is in competition with geminate recombination and ligand escape (see Figure 5), it is desirable to estimate the quantum yield for all three processes. Both geminate and bimolecular CO recombination processes shown in Figure 5 occur in many heme proteins. The yield of the geminate process is $\Phi_{geminate} = k_g/(k_e + k_g)$, where $k_{geminate}$ is k_g and k_{escape} is k_e as shown in the right-hand branch of Figure 5. In buffer solution at ambient temperature, the geminate yield for wild-type MbCO is 4%, while that for H93G(Im)CO is 15% (*1*). If the photolysis rate constant, $k_{h\nu}$, is greater than the bimolecular recombination rate constant, k_b, the deoxy species will be observed at steady state, provided the escape rate is much greater than the geminate recombination rate (i.e., $\Phi_{geminate} \ll 1$). The deoxy species is the bottleneck state in wild-type myoglobin MbCO because $k_e \approx 5 \times 10^6\ s^{-1} \gg k_g \approx 2 \times 10^5\ s^{-1} \gg k_b \approx 2 \times 10^3\ s^{-1}$ at 0.1 mM CO concentration (i.e., under pseudo-first-order conditions for CO)[4] (*35*). For a 1 mm × 100 μm cylindrically focused beam and 100 μM heme concentration, we calculate a photolysis rate of $k_{h\nu} \approx 3 \times 10^3\ s^{-1}$/mW of excitation light.[5] For 1 mW of excitation light in a spinning cell, the calculated photoalteration parameter is 0.07 (*36*). The observed photoproduct will be equal to the photoalteration parameter multiplied by the relative Raman scattering cross section $|\epsilon_{deoxy}/\epsilon_{CO}|^2 \approx 0.25$ m for excitation at 422.5 nm.[6] For example, under these conditions (1 mW at an excitation wavelength of 422.5 nm), the MbCO Raman spectrum observed experimentally has <5% detectable deoxy Mb* (data not shown). On the other hand, for a laser photolysis rate constant of $k_{h\nu} \approx 2 \times 10^4\ s^{-1}$ (corresponding to an intensity of 7 mW) the deoxy photoproduct is calculated to contribute ≈50% of the observed Raman scattering intensity

[4] The bimolecular rate constant $k \approx 2 \times 10^7\ M^{-1}\ s^{-1}$. For [CO] = 0.1 mM (corresponding to the 0.1 atm of CO pressure used in this study), $k' = k[CO] = 2 \times 10^3\ s^{-1}$.

[5] The photolysis rate in a stationary sample is $k_{h\nu} = I\sigma_A\phi$, where I is the flux (photons/cm^2), σ_A is the absorption cross section, and ϕ is the quantum yield. In the present case $\sigma_A = (3.824 \times 10^{-21})\epsilon$, where the extinction coefficient $\epsilon = 1.73 \times 10^5\ cm^{-1}\ M^{-1}$ for heme at the peak of the Soret band (λ = 420 nm). In a spinning cell, the cross section can be interpreted as a photoalteration parameter describing the fraction of the sample that is converted to photoproduct, $F = k_{h\nu}d/v$, where d is the beam waist and v is the linear velocity. For a 5 mm tube spinning at 300 Hz, the effective velocity is $v = 4.5\ ms^{-1}$. For a beam waist of 100 microns, we calculate $F = 0.07$.

(see Figure A3 in Supporting Information). However, when corrected for the relative Raman scattering cross section factor of $|\epsilon_{deoxy}/\epsilon_{CO}|^2 \approx 0.25$, the observed deoxy Mb photoproduct yield will be only 12.5%. In contrast to wild-type myoglobin, the photoproduct of photolyzed H93G(L)-CO is the CO-bound ground state for ligands such as pyridine and *N*-methylimidazole, pyridine and *N*-methylimidazole, where the geminate recombination rate constant, k_g, is greater than the ligand escape rate constant, k_e. The escape rate $k_e \approx 5 \times 10^6$ s^{-1} is not strongly affected by the ligand L in H93G(L)CO (*37*). The rapid geminate recombination explains the lack of change in the resonance Raman spectra for the H64V/H93G-CO photoproduct upon increasing laser intensity (Figure 4). The result of laser photolysis of H93G-CO in the absence of heterocyclic ligands resembles neither the wild-type deoxy Mb photoproduct nor the H93G/H64V-CO photoproduct. Figure 5 depicts a scheme where a His/H_2O ligand switch could compete with geminate recombination of H93G(His)CO and CO escape. We can quantify the competition between geminate recombination and a ligand switch by the ratio of the intensities of the two Fe−C stretching vibrations at 490 and 507 cm^{-1} to 520 cm^{-1} shown in Figure 2.[3] The 520 cm^{-1} band carries ≈40% of the intensity, suggesting that the steady-state fractional population of the six-coordinate H93G(H_2O)CO is ≈0.4.[7,8] A kinetic scheme is described in the Supporting Information.

Identity of the Histidine Ligand. There are two histidines, His64 and His97, located close enough to the heme iron (<5 Å) to ligate it in H93G-CO adducts. If the distal residue, His64, were to ligate the heme iron, then the CO stretching frequencies of H93G-CO shown in Figure 3 at 1963, 1943, and 1936 cm^{-1} would correspond to CO bound on the proximal side. Alternatively, if the proximal residue, His97, were the axial ligand, then the CO stretching frequencies of H93G-CO would correspond to CO bound in the distal pocket. The close correspondence of the observed frequencies for H93G-CO to the canonical A_0, A_1, and A_2 states of wild-type MbCO implies that CO is in the same environment in wild-type MbCO and H93G-CO (i.e., CO is bound in the distal pocket in both) (*20*, *21*, *38*−*40*). The H64V/H93G-CO double mutant was studied in order to test the functional role of H64. Since H64 is absent in the double mutant, proximal-bound CO should not be able to form a six-coordinate adduct. In fact, the strong similarity between the resonance Raman spectra of the H64V/H93G-CO mutant shown in Figure 4 and the H64V MbCO single mutant (data not shown) suggests that CO is bound on the distal side with a proximal H97 ligand. This hypothesis agrees with low-temperature FTIR studies that compare the CO stretching frequency in a number of H93G double mutants (*21*).

H93G-CO shows saturation behavior as a function of laser intensity as shown in Figure 2. H64V/H93G-CO Raman spectra are not dependent on laser intensity. This observation is consistent with a H97 proximal ligand with a rapid geminate recombination rate analogous to the H64V single mutant's rapid geminate recombination rate.

CONCLUSION

We have shown that dynamic ligand switching at the heme iron occurs in the H93G myoglobin model system. The driving force for the ligand switch is provided by the strong trans effect of CO favoring histidine in the six-coordinate complex and protein strain favoring H_2O ligation in the deoxy complex (*22*). The initial photoproduct of H93G(His)CO, H93G(His), is unstable. His dissociates to relieve strain in the protein backbone and is replaced by H_2O. CO recombination to the H93G(H_2O) complex is rapid, and the transient H93G(H_2O)CO species is observed by vibrational spectroscopy, providing strong evidence for the kinetic model. The cycle is completed and the equilibrium species reached by a ligand switch trans to CO, from H93G(H_2O)-CO to H93G(His)CO on the millisecond time scale. The fact that conformational strain can drive the dynamic ligand switch suggests that this model system is important for understanding ligation state changes in heme proteins (*5*−*7*, *13*).

ACKNOWLEDGMENT

S.F. acknowledges Los Alamos National Laboratory for support through a Director's Postdoctoral Fellowship. Many thanks to D. Barrick for helpful discussions.

SUPPORTING INFORMATION AVAILABLE

Raman and infrared spectra and a detailed kinetic analysis. This material is available free of charge via the Internet at http://pubs.acs.org.

REFERENCES

1. DePillis, G., Decatur, S. M., Barrick, D., and Boxer, S. G. (1994) *J. Am. Chem. Soc. 116*, 6981−6982.
2. Perutz, M. F. (1979) *Annu. Rev. Biochem. 48*, 327−386.
3. Nagai, K., Welborn, C., Dolphin, D., and Kitagawa, T. (1980) *Biochemistry 19*, 4755−4761.
4. Yu, A. E., Hu, S., Spiro, T. G., and Burstyn, J. N. (1994) *J. Am. Chem. Soc. 116*, 4117−4118.
5. Stone, J. R., and Marletta, M. A. (1994) *Biochemistry 33*, 5636−5640.
6. Williams, P. A., Fulop, V., Garman, E. F., Saunders, N. F. W., Ferguson, S. J., and Hajdu, J. (1997) *Nature 389*, 406−412.
7. Woodruff, W. H., Einarsdottir, O., Dyer, R. B., Bagley, K. A., Palmer, G., Atherton, S. J., Goldbeck, R. A., Dawes, T. D., and Kliger, D. S. (1991) *Proc. Natl. Acad. Sci. U.S.A. 88*, 2588−2592.
8. Spiro, T. G., Smulevich, G., and Su, C. (1990) *Biochemistry 29*, 4497−4508.

[6] Considering that the Soret band for the photoproduct is shifted from $\lambda_{max} = 420$ nm to $\lambda_{max} = 435$ nm, the observed yield of the deoxy photoproduct will be weighted by the relative resonance Raman scattering cross sections. These are proportional to the square of the ratio of the extinction coefficients $|\epsilon_{deoxy}/\epsilon_{CO}|^2 \approx 0.25$ at the laser wavelength of 422.5 nm. Thus, at steady state the relative amount of CO photoproduct observed is twice as great as the equilibrium H93G-(His)CO form.

[7] The relative intensities of the 490, 507, and 520 cm^{-1} bands were determined by fitting the line shape shown in the upper trace of Figure 2 to three Gaussians. The relative intensities are 0.29 ± 0.04:0.47 ± 0.06:1. The 520 cm^{-1} Raman band in the photoproduct represents the H93G(H_2O)CO population. Given the ratios determined from band fitting, this fraction is $1/(1 + 0.47 + 0.29) = 0.43 \pm 0.04$.

[8] This comparison includes only the A_1 substates for the equilibrium state compared to the photoproduct state. In addition to these A_1 substates at 1945 cm^{-1} for H93G(His)CO and 1960 cm^{-1} for H93G-(H_2O)CO, there are also substates A_2 at 1936 cm^{-1} and A_0 at 1967 cm^{-1} in MbCO, H93G(Im)CO, and H93G(His)CO. The H93G-CO spectrum may consist of an equilibrium between H93G(His)CO and H93G(H_2O)CO leading to the apparently larger A_0 peak for H93G-CO compared to H93G(Im)CO and to its shift from 1967 cm^{-1} in H93G(Im)CO and MbCO to 1963 cm^{-1} in H93G-CO.

9. Deinum, G., Stone, J. R., Babcock, G. T., and Marletta, M. A. (1996) *Biochemistry 35*, 1540−1547.
10. Kitagawa, T. (1988) in *Biological Applications of Raman Spectroscopy* (Spiro, T. G., Ed.).
11. Friedman, J., and Campbell, B. (1987) *Structural dynamics and reactivity in hemoglobin*, Springer-Verlag, New York, Berlin, Heidelberg, London, Paris, and Tokyo.
12. Sun, J., Loehr, T. M., Wilks, A., and Montellano, P. R. O. d. (1994) *Biochemistry 33*, 13734−13740.
13. Schelvis, J. P. M., Deinum, G., Varotsis, C. A., Ferguson-Miller, S., and Babcock, G. T. (1997) *J. Am. Chem. Soc. 119*, 8409−8416.
14. Barrick, D. (1994) *Biochemistry 33*, 6546−6554.
15. Decatur, S., DePillis, G. D., and Boxer, S. G. (1996) *Biochemistry 35*, 3925−3932.
16. Aono, S., Ohkubo, K., Matsuo, T., and Nakajima, H. (1998) *J. Biol. Chem. 273*, 25757−25764.
17. Shelver, D., Thorsteinsson, M. V., Kerby, R. L., Chung, S. Y., Roberts, G. P., Reynolds, M. F., Parks, R. B., and Burstyn, J. N. (1999) *Biochemistry 38*, 2669−2678.
18. Reynolds, M. F., Parks, R. B., Burstyn, J. N., Shelver, D., Thorsteinsson, M. V., Kerby, R. L., Roberts, G. P., Vogel, K. M., and Spiro, T. G. (2000) *Biochemistry 39*, 388−396.
19. Vogel, K. M., Spiro, T. G., Shelver, D., Thorsteinsson, M. V., and Roberts, G. P. (1999) *Biochemistry 38*, 2679−2687.
20. Decatur, S. M., and Boxer, S. G. (1995) *Biochem. Biophys. Res. Commun. 212*, 159−164.
21. Hu, R. B. (1999) Thesis, Stanford University, Stanford, CA.
22. Rougee, M., and Brault, D. (1975) *Biochemistry 14*, 4100−4106.
23. Teale, F. W. J. (1959) *Biochim. Biophys. Acta 35*, 543−547.
24. Omberg, K. M., Schoonover, J. R., Treadway, J. A., Leasure, R. M., Dyer, R. B., and Meyer, T. (1997) *J. Am. Chem. Soc. 119*, 7013−7018.
25. Franzen, S., Decatur, S., Boxer, S. G., Dyer, R. B., and Woodruff, W. H. (2000) *J. Phys. Chem. B 104*, 10359−10367.
26. Argade, P. V., Sassaroli, M., Rousseau, D. L., Inubushi, T., Ikeda-Saito, M., and Lapidot, A. (1984) *J. Am. Chem. Soc. 106*, 6593−6596.
27. Wells, A. V., Sage, T. J., Morikis, D., Champion, P. M., Chiu, M. L., and Sligar, S. G. (1991) *J. Am. Chem. Soc. 113*, 9655−9660.
28. Anderton, C. L., Hester, R. E., and Moore, J. N. (1997) *Biochim. Biophys. Acta 1338*, 107−120.
29. Ray, G. B., Li, X.-Y., Ibers, J. A., Sessler, J. L., and Spiro, T. G. (1994) *J. Am. Chem. Soc. 116*, 162−176.
30. Makinen, M. W., Houtchens, R. A., and Caughey, W. S. (1979) *Proc. Natl. Acad. Sci. U.S.A. 76*, 6042−6046.
31. Ansari, A., Berendzen, J., Braunstein, D., Cowen, B. R., Frauenfelder, H., Hong, M. K., Iben, I. E. T., Johnson, J. B., Ormos, P., Sauke, T. B., Scholl, R., Schulte, A., Steinbach, P. J., Vittitow, J., and Young, R. D. (1987) *Biophys. Chem. 26*, 337−355.
32. Smulevich, G., Mauro, J. M., Fishel, L. A., English, A. M., Kraut, J., and Spiro, T. G. (1988) *Biochemistry 27*, 5477−5485.
33. Argade, P. V., Ching, Y. C., and Rousseau, D. L. (1984) *Science 255*, 329−331.
34. Kerr, E. A., Mackin, H. C., and Yu, N. T. (1983) *Biochemistry 22*, 4373.
35. Henry, E. R., Sommer, J. H., Hofrichter, J., and Eaton, W. A. (1983) *J. Mol. Biol. 166*, 443−451.
36. Mathies, R., Oseroff, A. R., and Stryer, L. (1976) *Proc. Natl. Acad. Sci. U.S.A. 73*, 1−5.
37. Franzen, S., and Boxer, S. G. (1997) *J. Biol. Chem. 272*, 9655−9660.
38. Alben, J. O., Beece, D., Bowne, S. F., Doster, W., Eisenstein, L., Frauenfelder, H., Good, D., McDonald, J. D., Marden, M. C., Moh, P. P., Reinisch, L., Reynolds, A. H., Shyamsunder, E., and Yue, K. T. (1982) *Proc. Natl. Acad. Sci. U.S.A. 79*, 3744−3748.
39. Balasubramanian, S., Lambright, D. G., and Boxer, S. G. (1993) *Proc. Natl. Acad. Sci. U.S.A. 90*, 4718−4722.
40. Li, T. S., Quillin, M. L., Phillips, G. N., and Olson, J. S. (1994) *Biochemistry 33*, 1433−1446.

BI0023403